

RESEARCH ARTICLE

Molecular Bases of Catalysis and ADP-Ribose Preference of Human Mn^{2+} -Dependent ADP-Ribose/CDP-Alcohol Diphosphatase and Conversion by Mutagenesis to a Preferential Cyclic ADP-Ribose Phosphohydrolase

Alicia Cabezas¹, João Meireles Ribeiro¹, Joaquim Rui Rodrigues², Iralis López-Villamizar¹, Ascensión Fernández¹, José Canales¹, Rosa María Pinto¹, María Jesús Costas¹, José Carlos Cameselle^{1*}

1 Grupo de Enzimología, Departamento de Bioquímica y Biología Molecular y Genética, Facultad de Medicina, Universidad de Extremadura, Badajoz, Spain, **2** Escola Superior de Tecnologia e Gestão, Instituto Politécnico de Leiria, Leiria, Portugal

* camselle@unex.es



OPEN ACCESS

Citation: Cabezas A, Ribeiro JM, Rodrigues JR, López-Villamizar I, Fernández A, Canales J, et al. (2015) Molecular Bases of Catalysis and ADP-Ribose Preference of Human Mn^{2+} -Dependent ADP-Ribose/CDP-Alcohol Diphosphatase and Conversion by Mutagenesis to a Preferential Cyclic ADP-Ribose Phosphohydrolase. PLoS ONE 10(2): e0118680. doi:10.1371/journal.pone.0118680

Academic Editor: Danilo Roccatano, Jacobs University Bremen, GERMANY

Received: October 15, 2014

Accepted: January 6, 2015

Published: February 18, 2015

Copyright: © 2015 Cabezas et al. This is an open access article distributed under the terms of the [Creative Commons Attribution License](https://creativecommons.org/licenses/by/4.0/), which permits unrestricted use, distribution, and reproduction in any medium, provided the original author and source are credited.

Data Availability Statement: DNA and protein sequences are deposited in GenBank under accession numbers KF880964 and AHG56452. The rest of relevant data are within the paper and its Supporting Information files.

Funding: The work was supported by grants from the Ministerio de Ciencia e Innovación del Gobierno de España (BFU2009-07296), and from the Junta de Extremadura or Gobierno de Extremadura (GRU09135, GR10133), cofinanced by Fondo

Abstract

Among metallo-dependent phosphatases, ADP-ribose/CDP-alcohol diphosphatases form a protein family (ADPRibase-Mn-like) mainly restricted, in eukaryotes, to vertebrates and plants, with preferential expression, at least in rodents, in immune cells. Rat and zebrafish ADPRibase-Mn, the only biochemically studied, are phosphohydrolases of ADP-ribose and, somewhat less efficiently, of CDP-alcohols and 2',3'-cAMP. Furthermore, the rat but not the zebrafish enzyme displays a unique phosphohydrolytic activity on cyclic ADP-ribose. The molecular basis of such specificity is unknown. Human ADPRibase-Mn showed similar activities, including cyclic ADP-ribose phosphohydrolase, which seems thus common to mammalian ADPRibase-Mn. Substrate docking on a homology model of human ADPRibase-Mn suggested possible interactions of ADP-ribose with seven residues located, with one exception (Cys²⁵³), either within the metallo-dependent phosphatases signature (Gln²⁷, Asn¹¹⁰, His¹¹¹), or in unique structural regions of the ADPRibase-Mn family: s2s3 (Phe³⁷ and Arg⁴³) and h7h8 (Phe²¹⁰), around the active site entrance. Mutants were constructed, and kinetic parameters for ADP-ribose, CDP-choline, 2',3'-cAMP and cyclic ADP-ribose were determined. Phe³⁷ was needed for ADP-ribose preference without catalytic effect, as indicated by the increased ADP-ribose K_m and unchanged k_{cat} of F37A-ADPRibase-Mn, while the K_m values for the other substrates were little affected. Arg⁴³ was essential for catalysis as indicated by the drastic efficiency loss shown by R43A-ADPRibase-Mn. Unexpectedly, Cys²⁵³ was hindering for cADPR phosphohydrolase, as indicated by the specific tenfold gain of efficiency of C253A-ADPRibase-Mn with cyclic ADP-ribose. This allowed the design of a triple mutant (F37A+L196F+C253A) for which cyclic ADP-ribose was the best substrate, with a catalytic efficiency of $3.5 \cdot 10^4 M^{-1}s^{-1}$ versus $4 \cdot 10^3 M^{-1}s^{-1}$ of the wild type.

Europeo de Desarrollo Regional and Fondo Social Europeo. The funders had no role in study design, data collection and analysis, decision to publish, or preparation of the manuscript.

Competing Interests: The authors have declared that no competing interests exist.

Introduction

The Mn^{2+} -dependent ADP-ribose/CDP-alcohol diphosphatase (ADPRibase-Mn; EC 3.6.1.53) is one of several enzymes known in mammals to hydrolyze with some degree of specificity the phosphoanhydride linkage of ADP-ribose and other nucleoside diphosphate-X (NDP-X) compounds [1, 2]. Two important peculiarities of ADPRibase-Mn, studied in the rat enzyme, are its marked preference for Mn^{2+} over Mg^{2+} as the activating cation, with a requirement of low micromolar Mn^{2+} for activity [1, 2], which is near the physiological level of the metal in animal cells [3], and its minor but unique activity on the phosphoanhydride linkage of cyclic ADP-ribose (cADPR) [4].

The ADPRibase-Mn substrates ADP-ribose and cADPR are intracellular signal molecules with known effects on TRPM2 ion channels [5–9] or, in the case of cADPR, on ryanodine receptors [10–12]. Both are putatively formed, in mammals, from NAD^+ by CD38 and Bst-1/CD157 (reviewed in [13]). The calcium regulator cADPR is an analog of ADP-ribose in which adenine, besides the standard N9-glycosydic linkage with the C1' atom of the adenosine moiety, establishes also a N1-glycosydic linkage with the C1'' atom of the other ('northern') ribose, thus forming a macrocyclic structure [12]. In some animals, like *Aplysia*, cADPR synthesis is catalyzed from NAD^+ by an ADP-ribosyl cyclase specifically acting as such [14–16], although in mammals it is synthesized by a quantitatively minor alternative pathway of the NAD glycohydrolases CD38 and Bst-1/CD157, that mainly hydrolyze NAD^+ to ADP-ribose. [17–24]. In mammals, the turnover of cADPR signaling is exerted also by CD38 and Bst-1/CD157, which convert cADPR to ADP-ribose by hydrolysis of the N¹-glycosidic linkage [17–19, 21, 23]. The diphosphate group of cADPR is resistant to phosphohydrolases of broad specificity [4, 18, 25], like snake venom phosphodiesterase which otherwise hydrolyzes a large variety of 5'-nucleotide phosphodiester or phosphoanhydride derivatives including e.g. ADP-ribose [26–28]. It is thus remarkable that rat ADPRibase-Mn acts as cADPR phosphohydrolase with low but significant efficiency (about 100-fold lower than the activity on ADP-ribose), yielding N¹-(5-phosphoribosyl)-AMP as the product. This could hypothetically represent a novel route for cADPR turnover [4]. Interestingly, cADPR and its product of hydrolysis by ADPRibase-Mn, N¹-(5-phosphoribosyl)-AMP, have been identified in a metabolomic profile of human erythrocytes infected with *Plasmodium falciparum* [29]. Also interestingly, in the search for pharmacologically-active cADPR analogs [30–33], the previously overlooked possibility of cADPR phosphohydrolysis is now being taken into account [34–36].

The taxonomic distribution of ADPRibase-Mn is intriguing, as it has been reported to be restricted, among eukaryotes, to vertebrates and plants [2]. Furthermore, biochemical and in-silico expression data indicate that ADPRibase-Mn is preferentially expressed in immune cells of rodents [2, 37]. Related to this pattern, it is worth recalling that CD38 and Bst-1/CD157, the proteins that form ADP-ribose and cADPR, have a regulatory role at the interface between the innate and the adaptative immune systems [38–41]. In this field there are still some incompletely solved issues. One is the so-called topological paradox posed by the location of mammalian proteins forming ADP-ribose and cADPR in the outer surface of plasma membrane, against the cytosolic action of these compounds. Several explanatory mechanisms for this apparent paradox have been advanced [12, 42–45]. The intracellular termination of these two signals and of their effects is also worth of consideration. In addition to ADPRibase-Mn, two mammalian enzymes of the Nudix superfamily are known that can efficiently hydrolyze ADP-ribose [1, 46–49]. However, for the turnover of cADPR, as stated above, only its conversion to ADP-ribose by the glycohydrolytic activity of CD38 and Bst-1/CD157, i.e. the same membrane proteins responsible for its synthesis, is generally mentioned. Therefore, it remains to be seen

whether ADPRibase-Mn could be involved in this regulatory network with a role in the turnover of cADPR [4].

ADPRibase-Mn proteins belong to the metallo-dependent phosphatases (MDP) SCOP2 superfamily, within which they form a structural family of their own (ADPRibase-Mn-like; ID 4002589) [50]. In the CATH classification, ADPRibase-Mn proteins form also a unique functional family within the structural cluster SC:2 of superfamily 3.60.21.10 [51]. The only ADPRibase-Mn enzymes that have been biochemically studied are those from rat [1, 2, 4] and zebrafish [52]. The structure of zebrafish ADPRibase-Mn in complex with P_i is deposited in Protein Data Bank (PDB ID 2NXF), and it has been used as template to construct homology models of murine and human proteins [53]. Like other MDPs, the putative active site of ADPRibase-Mn contains a dimetallic center, possibly Fe/Mn, as indicated for the zebrafish ADPRibase-Mn (<http://www.uwstructuralgenomics.org/gallery/2nxf.pdf> [54]).

Concerning substrate specificity, ADPRibase-Mn enzymes are Mn^{2+} -dependent ADP-ribose/CDP-alcohol diphosphatases that hydrolyze the phosphoanhydride linkage of ADP-ribose and, somewhat less efficiently, of CDP-choline, CDP-glycerol and CDP-ethanolamine. The catalytic efficiency of ADP-ribose hydrolysis, depending on the enzyme source (rat or zebrafish), is 4–60-fold higher than that of CDP-alcohol hydrolysis, and it is a reflection of the low K_m value for ADP-ribose, in spite of the higher k_{cat} shown for CDP-alcohols in every case [2, 52]. Besides the diphosphatase activities on ADP-ribose and CDP-alcohols, ADPRibase-Mn enzymes display also activity on ADP and 2',3'-cAMP with similar or lower efficiency than on CDP-alcohols, and as stated above the rat enzyme is able to hydrolyze the phosphoanhydride linkage of cADPR. The overall specificity of ADPRibase-Mn enzymes is highlighted by their lack of significant activity towards ADP-glucose, UDP-glucose, CDP-glucose, CDP, CMP, AMP or 3',5'-cAMP [1, 2, 52]. In contrast to the rat enzyme, zebrafish ADPRibase-Mn does not hydrolyze cADPR significantly, being in this concern at least 150-fold less efficient than the rat enzyme, while both of them are equally efficient on ADP-ribose [52]. Therefore, it remains to be established whether the cADPR phosphohydrolase activity is a peculiarity of rat ADPRibase-Mn or may be shared at least by enzymes from other mammalian sources.

The molecular basis of ADPRibase-Mn specificity in terms of interactions between substrates and protein has not been so far investigated by mutagenesis. In the present work, we have aimed to understand the catalytic behavior of human ADPRibase-Mn by performing an extensive mutagenesis study based on substrate docking simulations. Important questions are answered on the molecular basis of the enzyme preference for ADP-ribose and the cADPR phosphohydrolase activity of mammalian members of the ADPRibase-Mn-like family. Interestingly, a triple mutant of human ADPRibase-Mn acts preferentially as cADPR phosphohydrolase, due to an increased catalytic efficiency on cADPR and decreased efficiencies on other substrates.

Materials and Methods

Materials

The sources of the products used, including cADPR purified from the commercial preparation, were as described elsewhere [2, 4, 52].

Cloning and sequencing of human ADPRibase-Mn cDNA

The open reading frame (ORF) of human ADPRibase-Mn was cloned from human liver cDNA (Marathon-Ready cDNA, Clontech) by PCR. The primers were based on the *ADPRM* mRNA accession no. NM_020233, which codes for the hypothetical 342-aa protein NP_064618, that is 86% and 51% identical with the biochemically-studied ADPRibase-Mn enzymes from rat

(ABW03224 [2, 4]) and zebrafish (2NXF_A [52]), respectively. The sequence of the forward primer was CTAGCGTCGACATGGATGATAAACCCAACCCTGAAGCCC, which includes a SalI site (single underline) preceding the ORF initiation codon (double underline); and that of the reverse primer was CAGGTGCGGCCCTAACCAATGGAATGCTCTTTCTTTC, which includes a NotI site (single underline) after the stop codon (double underline). The amplicon was first cloned in pGEM-T Easy vector by T/A ligation and, after identification of a clone with the expected insert, it was excised and subcloned in frame with the glutathione S-transferase (GST) tag of the pGEX-6P-3 vector cut with NotI and SalI, yielding plasmid pGEX-6P-3-hADPRM. The 1029-nt sequence of the human ORF insert was confirmed by double-strand sequencing (Servicio de Genómica, Instituto de Investigaciones Biomédicas Alberto Sols, Consejo Superior de Investigaciones Científicas-Universidad Autónoma de Madrid, Madrid) and deposited in GenBank with accession number KF880964. It coincided with the ORF included in mRNA NM_020233, except for the silent substitutions C18T and A1017C due to primer design. The theoretical translation of the cloned ORF (accession number AHG56452) was thus fully identical to the hypothetical 342-aa protein NP_064618.

Site-directed mutagenesis

Point mutants were constructed following the *QuikChange* protocol (Stratagene) using mutagenic primer pairs and pGEX-6P-3-hADPRM as template. The double mutants were constructed starting from pGEX-6P-3-F37A-hADPRM, and the triple one from pGEX-6P-3-F37A+L196F-hADPRM. The forward mutagenic primers are shown in [S1 Table](#); the reverse primers were the exact reverse complement of those. The correctness of all the mutants was confirmed by double-strand sequencing of the complete coding sequence as above.

Expression and purification of human ADPRibase-Mn protein and its mutant forms

The wild type and mutant proteins were expressed as fusions with glutathione S-transferase (GST) from pGEX-6P-3-hADPRM or the corresponding mutated plasmid. The recombinant proteins were purified by affinity chromatography on glutathione-Sepharose 4B (GE Healthcare), and separated from the GST tag by specific proteolysis with the PreScission protease [2]. This yielded each protein with an 11-amino acid N-terminal extension (GPLGSPNSRVD). Protein concentration was assayed in the final preparations according to Bradford [55] and the purity was estimated by SDS-PAGE stained with Coomassie Blue followed by quantitation by image analysis with the GelAnalyzer 2010 software (<http://www.gelanalyzer.com>; last access on December 2, 2014). In all cases, a single major protein band of ≈ 40.5 kDa, the approximate expected size for recombinant ADPRibase-Mn and its mutants, was observed. It accounted in the different preparations for 52%–79% of protein in the gel lanes. The estimations of purity for each protein are summarized in [S2 Table](#). Since the wild type ADPRibase-Mn was 70% pure, the purity ratios of the mutants versus the wild type ranged 0.74–1.13. So the minor differences of purity between some of the mutants and the wild type do not affect to an important extent the estimation of the shifts of k_{cat} and k_{cat}/K_m elicited by the mutations.

Enzyme assays

All the enzyme assays and kinetic studies were as described elsewhere, and were linear with time and ADPRibase-Mn amount [4, 52]. In summary, phosphohydrolytic reactions were studied by measuring colorimetrically the P_i liberated by alkaline phosphatase from the reaction products, with the exceptions of the phosphohydrolytic reactions of CDP, CMP, ADP and AMP, for which the P_i liberated was measured without including alkaline phosphatase in the

assay, and of cADPR phosphohydrolysis which was studied by following the accumulation of N^1 -(5-phosphoribosyl)-AMP by HPLC (see below). Under the standard conditions, the assays were conducted at 37°C, pH 7.5, and in the presence of 5 mM $MnCl_2$, unless otherwise stated. Saturation analysis was conducted from initial-rate assays. The k_{cat} and K_m values were obtained by nonlinear regression of the Michaelis-Menten equation to the experimental data points using the Solver tool of the Microsoft Excel 2004 for the Mac version 11.0. In cases where separate k_{cat} and K_m values could not be estimated, the k_{cat}/K_m ratio (catalytic efficiency) was calculated from initial-rate assays at low substrate when velocity is proportional to substrate concentration (S) and the enzyme is largely unbound to substrate. Under these conditions $k_{cat}/K_m = v/(E S)$, E being the total enzyme concentration [56].

High performance liquid chromatography

A HP-1100 chromatograph (Hewlett-Packard) was used with a manual injector equipped with a 20- μ l injection loop and a diode array detector. The analyses were performed by ion-pair reverse-phase HPLC in a 15 cm x 0.4 cm octadecylsilica column (Kromasil 100; Teknokroma, Sant Cugat del Vallés, Barcelona, Spain) with a 1 cm x 0.4 cm pre-column of the same material. The chromatographic conditions for analyses of enzyme reaction products were as described for the hydrolysis of cADPR [4] or 2',3'-cAMP [52]. Chromatogram analyses were performed with the HP ChemStation software.

Sequence analyses

Searches for eukaryotic ADPRibase-Mn homologs were done by BlastP analyses [57], using the human protein as query, against NCBI_nr or NCBI_RefSeq databases (last access on July 7, 2014) [58]. The former was used to test for the absence of homologous proteins in specific taxonomic groups; the latter was mainly used to retrieve a set of representative homologous proteins for sequence alignment. This set of proteins was prepared such that (i) only one protein per species was included (the one with lower E value when compared with human ADPRibase-Mn); (ii) proteins with an identity higher than 95% with any other already selected were discarded (in order to avoid overrepresentation of particular taxonomic groups); (iii) proteins with less than an 80% of query coverage or without the complete MDP-superfamily motif (DX [H/X]-X_n-GDXX[D/X]-X_n-GNH[D/E]-X_n-[G/X]H-X_n-GHX[H/X] [59–63]) were also discarded. Protein alignments were performed with Clustal Omega [64] using default parameters and analyzed and colored with ESPript [65].

Homology model of human ADPRibase-Mn

The coordinates of the homology model of human ADPRibase-Mn were downloaded on July 24, 2011 from the SWISS-MODEL repository [53]. This model is based on the known structure of zebrafish ADPRibase-Mn (Protein Data Bank ID 2NXF), with which the human protein has 66% similarity, including 51% identity. The template and the downloaded model lacked the fourteen N-terminal and the six C-terminal residues, so to obtain a complete model they were built with Modeller [66]. The coordinates for the two metal ions and the water molecule coordinated with them were taken from the structure of zebrafish ADPRibase-Mn.

Substrate docking

The model of ADPRibase-Mn and its ligands were prepared for docking as described [2, 4, 52]: the ligand coordinates were generated with Marvin (Chemaxon), the receptor and the ligands were prepared for docking with AutoDock Tools [67] and docking calculations were run with

AutoDock [68]. Two hundred conformations were obtained for each substrate docked, except that 1000 conformations were obtained for cADPR. For selection of the best docked conformations, it was hypothesized that the metal-bridging water could act as the attacking nucleophile over the P atom participating in the substrate scissile bond, like in the mechanisms of other phosphoesterases [61, 69]. For ADP-ribose, CDP-choline and cADPR, the best conformation was taken as the one with the lowest energy level among those in which the angle formed by the O-to-P attack line and the scissile P-O bond was $\geq 170^\circ$. For 2',3'-cAMP, which posed in two different orientations favoring either 3'-AMP or 2'-AMP as product, the conformation chosen had the largest attack angle among those showing the orientation favorable to 3'-AMP formation. In agreement with the above mentioned hypothesis, one of the substrate P atoms was at short distance ($< 3 \text{ \AA}$) of the metal-bridging water oxygen in all the selected conformations. The coordinates of the four docking complexes with the model structure of human ADPRibase-Mn are included in [S1–S4 Dataset](#).

Molecular dynamics simulations

The complex of human ADPRibase-Mn with ADP-ribose obtained by docking was the starting structure for the simulation of molecular dynamics (MD) of the enzyme-substrate complex and the free enzyme (after ADP-ribose removal). Geometry optimizations and MD simulations were performed with the GROMACS package (version 4.0.5) [70] in combination with the GROMOS 53A6 force field [71]. For the simulation of the enzyme-substrate complex, force field parameters for ADP-ribose were assigned based on analogous functional groups already present in the force field library. Each system was immersed in a cubic box of SPC water molecules [72] and 50 mM NaCl. The minimum distance between the protein and the walls of the periodic box was 10 \AA . The energy of each system was minimized with 2000–2500 steps of steepest descent algorithm. Equilibration was carried out in three steps: first, 20 ps of constant volume equilibration were performed at 300 K with position restraints on the protein; second, 200 ps of constant pressure equilibration with position restraints on the protein; third, 100 ps of constant pressure equilibration without position restraints. Production runs were started at this point. Bond lengths of protein (and ligand) were constrained with LINCS [73, 74] and those of water with SETTLE [75], allowing for a 2-fs time step. The non-bonded interactions were treated with a triple-range schema with cut-off radii of 8 \AA and 14 \AA . The short-range van der Waals and electrostatic interactions were evaluated every time step from a pairlist that was generated every five steps. Medium-range van der Waals and electrostatic interactions (between 8 \AA and 14 \AA) were computed every fifth step and kept constant between pairlist updates. Long-range electrostatic interactions outside the longer cut-off were accounted for by a reaction field with a relative dielectric permittivity of 66. The temperature (300 K) and pressure (1 atm) were kept constant using the Berendsen thermostat and barostat [76] with $\tau_T = 0.1 \text{ ps}$ and $\tau_P = 0.5 \text{ ps}$, respectively. Coordinates were saved every 1 ps. To help maintaining the geometry of the dimetallic center, the distances between the metal ions and the coordinated water molecule were constrained to their initial distances.

Results and Discussion

Catalytic specificity of human ADPRibase-Mn including cADPR phosphohydrolase activity

The catalytic specificity of the recombinant protein was as expected for a typical ADPRibase-Mn [1, 52]. When phosphohydrolytic activities were assayed in the presence of 5 mM Mn^{2+} , at a fixed 500 μM substrate concentration, ADP-ribose was hydrolyzed at the highest rate. The

CDP-alcohols (CDP-choline, CDP-ethanolamine and CDP-glycerol) followed near at 70%–90% of the ADP-ribose rate. Somewhat slower (40%) was the hydrolysis of 2',3'-cAMP, and even slower the reactions of ADP and cADPR. ADP-glucose, UDP-glucose, CDP, CMP, AMP, 3',5'-cAMP were not hydrolyzed at detectable rates (< 0.1%). The results are summarized in [S3 Table](#).

The reaction product of 2',3'-cAMP hydrolysis, assayed by HPLC, was mainly 3'-AMP, which corresponds to the hydrolysis of the ester linkage on the 2'-O side of the phosphodiester, although a minor proportion of 2'-AMP was also formed (< 3% of 3'-AMP), like with zebrafish ADPRibase-Mn [52]. The product of cADPR hydrolysis, also assayed by HPLC, was N^1 -(5-phosphoribosyl)-AMP, which corresponds to the hydrolysis of the phosphoanhydride linkage of cADPR like with rat ADPRibase-Mn [4].

The responses of activity to varying pH or Mn^{2+} concentration were studied with ADP-ribose, CDP-choline and 2',3'-cAMP. The hydrolysis of ADP-ribose, assayed at pH 6.0–10.5, showed a symmetrical bell-shaped profile with maximal activity at pH 8.5, whereas the hydrolysis of the other substrates showed a rather flat profile at pH 6.0–8.5 followed by a steep decrease at higher pH values ([S1 Fig.](#)). This behavior is similar to that shown by both the rat and the zebrafish ADPRibase-Mn [2, 52]. The different pH-activity profiles seem to indicate that the hydrolysis of ADP-ribose, but not the other substrates, depend on the dissociation of an acidic group with apparent pK_a between 7 and 8. The responses of activity to Mn^{2+} were near complete at about 10 μM metal and remained essentially without change up to 5 mM ([S2 Fig.](#)), similarly to the rat ADPRibase-Mn [1, 2].

Saturation kinetics at varying concentrations of substrate, with Mn^{2+} concentration fixed at 5 mM and at pH 7.5, was studied with ADP-ribose, CDP-choline, 2',3'-cAMP and cADPR. The best substrate in terms of catalytic efficiency (k_{cat}/K_m) was ADP-ribose due to its lower K_m value, followed by CDP-choline, 2',3'-cAMP and cADPR ([Table 1](#)). The phosphoanhydride linkage of cADPR was hydrolyzed with the same catalytic efficiency as the rat enzyme [4], i.e. about 4000 $M^{-1}s^{-1}$, which is at least 150-fold higher than the efficiency of the zebrafish enzyme [52]. The difference was due to the much higher k_{cat} values of the mammalian enzymes for this substrate, compared to the enzyme from the fish. This confirmed that a relatively robust cADPR phosphohydrolase activity may be a general feature of mammalian ADPRibase-Mn. In this concern, and as earlier pointed out, a ratio of efficiencies for ADP-ribose/cADPR hydrolysis near 100 ([Table 1](#) and [4]) is near the ratio of ADP-ribose/cADPR synthesis from NAD by CD38, the major cADPR-forming enzyme in mammals [15, 18, 20, 77]. Therefore, the potential of ADPRibase-Mn for cADPR turnover may be relevant.

Reexamination of the taxonomic distribution of the ADPRibase-Mn-like family

It has been reported that, among animals, the ADPRibase-Mn-like protein family has a phylogenetic distribution restricted to vertebrates, although it is present also in plants and algae [2]. This distribution was here reexamined to account for the considerable increase in database size since that report, and to test the degree of conservation of important residues revealed by the present study (see below). The results confirmed essentially the above-mentioned distribution with minor but perhaps important exceptions. ADPRibase-Mn proteins appeared widespread in vertebrates (possibly also in other Chordata and in Hemichordata) and plants, were absent from fungi, and irregularly distributed among protists. Concerning invertebrates, significant ADPRibase-Mn relatives were absent from most taxa, which included those with some organism(s) with well characterized genomes, like Arthropoda, Echinodermata and Nematoda. However, there was the important exception of Mollusca, where ADPRibase-Mn-like proteins

Table 1. Kinetic parameters of human ADPRibase-Mn and mutants.

Mutations	Substrate	k_{cat}		K_m		k_{cat}/K_m	
		s^{-1}	Fold change	μM	Fold change	$M^{-1}s^{-1}$	Fold change
Wild type	ADP-ribose	35 ± 11	–	60 ± 8	–	590000 ± 160000	–
	CDP-choline	50 ± 4	–	350 ± 60	–	150000 ± 30000	–
	2',3'-cAMP	60 ± 13	–	2400 ± 300	–	25000 ± 6000	–
	cADPR	3.2 ± 0.2	–	780 ± 200	–	4000 ± 1000	–
Q27H	ADP-ribose	10 ± 3	↓4	200 ± 14	↑3	52000 ± 10000	↓11
	CDP-choline	39 ± 12	≈	2700 ± 200	↑8	14000 ± 3000	↓11
	2',3'-cAMP	4.3 ± 1.1	↓14	2300 ± 130	≈	1900 ± 400	↓13
	cADPR	na	na	na	na	150 ± 20	↓27
F37A	ADP-ribose	14 ± 3	↓3	1150 ± 80	↑19	12000 ± 2000	↓50
	CDP-choline	33 ± 7	↓1.5	970 ± 140	↑3	34000 ± 3000	↓4
	2',3'-cAMP	36 ± 6	↓1.7	5100 ± 300	↑2	7000 ± 700	↓4
	cADPR	na	na	na	na	1300 ± 200	↓3
F37Y	ADP-ribose	50 ± 11	≈	77 ± 10	≈	650000 ± 170000	≈
	CDP-choline	76 ± 23	≈	430 ± 50	≈	180000 ± 60000	≈
	2',3'-cAMP	70 ± 18	≈	2500 ± 180	≈	28000 ± 5000	≈
	cADPR	na	na	na	na	4100 ± 100	≈
R43A	ADP-ribose	0.003 ± 0.003	↓12000	115 ± 30	↑1.9	30 ± 30	↓20000
	CDP-choline	0.025 ± 0.004	↓2000	9000 ± 8000	↑26	6 ± 6	↓25000
	2',3'-cAMP	0.95 ± 0.14	↓60	7600 ± 1900	↑3	130 ± 20	↓200
	cADPR	na	na	na	na	0.1 ± 0.1	↓40000
N110A	ADP-ribose	4.3 ± 0.6	↓8	290 ± 50	↑5	15000 ± 200	↓40
	CDP-choline	5.7 ± 1.4	↓9	4000 ± 1100	↑11	1500 ± 400	↓100
	2',3'-cAMP	0.11 ± 0.01	↓550	1050 ± 60	↓2	100 ± 10	↓250
	cADPR	na	na	na	na	130 ± 30	↓31
H111A	ADP-ribose	0.47 ± 0.08	↓75	140 ± 14	↑2	3000 ± 200	↓200
	CDP-choline	2.2 ± 0.2	↓23	7500 ± 700	↑21	300 ± 30	↓500
	2',3'-cAMP	7.4 ± 2.9	↓8	1250 ± 450	↓2	6000 ± 400	↓4
	cADPR	na	na	na	na	70 ± 6	↓60
H111N	ADP-ribose	2.3 ± 0.2	↓15	78 ± 5	≈	29000 ± 4000	↓20
	CDP-choline	5.3 ± 1.0	↓9	2700 ± 500	↑8	2000 ± 400	↓75
	2',3'-cAMP	34 ± 6	↓1.8	1800 ± 450	≈	19000 ± 2000	≈
	cADPR	na	na	na	na	290 ± 40	↓14
L196A	ADP-ribose	16 ± 4	↓2	130 ± 5	↑2	120000 ± 30000	↓5
	CDP-choline	29 ± 13	↓1.7	470 ± 90	≈	62000 ± 20000	↓2
	2',3'-cAMP	30 ± 10	↓2	3400 ± 500	≈	9000 ± 4000	↓3
	cADPR	na	na	na	na	900 ± 100	↓4
F210A	ADP-ribose	19 ± 3	↓1.8	2100 ± 100	↑34	9000 ± 1000	↓70
	CDP-choline	50 ± 12	≈	11000 ± 2600	↑32	4000 ± 100	↓40
	2',3'-cAMP	2.7 ± 0.2	↓22	7600 ± 1700	↑3	400 ± 10	↓60
	cADPR	na	na	na	na	8 ± 1	↓500
C253A	ADP-ribose	97 ± 8	↑3	94 ± 6	↑1.6	1000000 ± 100000	↑1.7
	CDP-choline	79 ± 7	↑1.6	500 ± 70	≈	160000 ± 20000	≈
	2',3'-cAMP	83 ± 5	≈	2600 ± 250	≈	32000 ± 2000	≈
	cADPR	8.9 ± 0.8	↑3	200 ± 40	↓4	44000 ± 9000	↑11

(Continued)

Table 1. (Continued)

Mutations	Substrate	k_{cat}		K_m		k_{cat}/K_m	
		s^{-1}	Fold change	μM	Fold change	$M^{-1}s^{-1}$	Fold change
F37A+L196A	ADP-ribose	7 ± 2	↓5	1150 ± 500	↑19	6000 ± 2000	↓100
	CDP-choline	25 ± 5	↓2	1250 ± 250	↑4	21000 ± 8000	↓7
	2',3'-cAMP	19 ± 2	↓3	4800 ± 900	↑2	4000 ± 1000	↓6
	cADPR	na	na	na	na	900 ± 100	↓4
F37A+L196F	ADP-ribose	8 ± 1	↓4	1600 ± 100	↑26	4800 ± 200	↓120
	CDP-choline	26 ± 3	↓1.9	1500 ± 250	↑4	17000 ± 3000	↓9
	2',3'-cAMP	28 ± 3	↓2	7100 ± 650	↑3	3900 ± 400	↓6
	cADPR	na	na	na	na	1600 ± 200	↓3
F37A+L196F+C253A	ADP-ribose	13 ± 1	↓3	1200 ± 230	↑20	11000 ± 1700	↓50
	CDP-choline	37 ± 5	≈	1700 ± 120	↑5	22000 ± 2600	↓7
	2',3'-cAMP	20 ± 3	↓3	5200 ± 1000	↑2	4000 ± 800	↓6
	cADPR	16 ± 3	↑5	460 ± 120	↓1.7	35500 ± 4300	↑9

The values with S.D. are averages of at least three experiments. Fold change was calculated with respect to the parameters of the wild type. ≈, change < 1.5 fold; na, not assayed (in these cases k_{cat}/K_m was calculated from initial-rate assays at low substrate when velocity was proportional to substrate concentration; see under [Materials and Methods](#)).

doi:10.1371/journal.pone.0118680.t001

seem to occur in Gastropoda (*Aplysia californica* and *Lottia gigantea*) and Bivalvia (*Crassostrea gigas*). A significant homolog was also found in Annelida (*Helobdella robusta*). Of course, it remains to be seen whether these proteins have ADPRibase-Mn enzyme activities. A summary of the current view of this protein family is shown in [S3 Fig](#), under the form of a sequence alignment.

Identification of amino acids interacting with ADP-ribose in the model structure of the enzyme-substrate complex and their relationship to defined regions of human ADPRibase-Mn

The ADPRibase-Mn family contains the disperse motif of the MDP superfamily that responds to the description DX[H/X]-X_n-GDXX[D/X]-X_n-GNH[D/E]-X_n-[G/X]H-X_n-GHX[H/X], i.e. five short consensus regions separated by long tracts (X_n) of nonconserved sequence that, however, form a well conserved structure. The five short conserved regions are marked in [Fig. 1](#), [Fig. 2](#) and [S3 Fig](#). They are part of loops located at the end of β strands and contains the amino acids that form the dinuclear center by coordination to the metals [59–63]. Other than the MDP superfamily motif, very little sequence conservation is found when the ADPRibase-Mn-like family is compared to the other eleven MDP families classified in SCOP2. However, there is ample and strong conservation of structure throughout the superfamily. Against this background, three structural elements stand out as unique to the ADPRibase-Mn-like family: using the numbering of zebrafish protein sequence, they correspond approximately to amino acids 20–35, 65–70 and 150–195 [52]. These will be here named, respectively, regions s2s3, h2, and h7h8, according to the secondary structure elements (s, strand; h, helix) of zebrafish ADPRibase-Mn that they contain. These unique regions delimit the entrance to the active site of zebrafish ADPRibase-Mn and of the homology models for which it served as template. They are present throughout the ADPRibase-Mn-like family with a significant degree of sequence conservation ([S3 Fig](#)), and they are candidates to contain substrate specificity determinants.

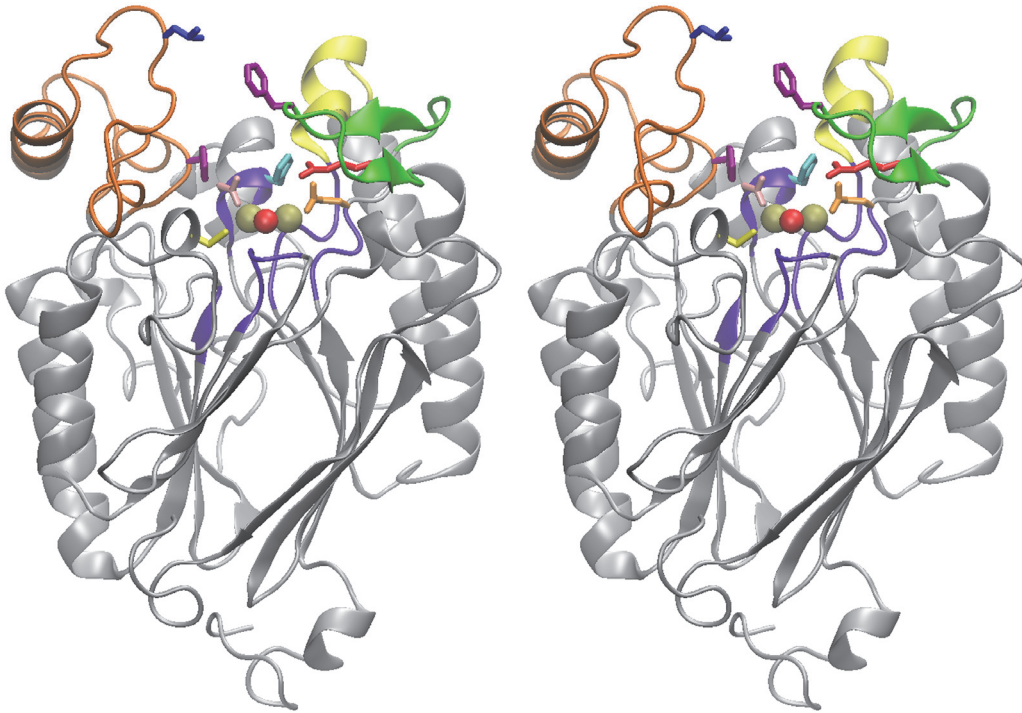


Fig 1. Stereogram of the model structure of human ADPRibase-Mn. Schematic model without substrate, showing metals (golden spheres), metal-bridging water (red sphere), the five short consensus regions of the MDP-superfamily motif (violet), and the ADPRibase-Mn unique regions s2s3 (green), h2 (yellow), and h7h8 (orange). The amino acids chosen for mutagenesis are highlighted and colored by residue: Gln²⁷ (orange), Phe³⁷ (magenta; in s2s3), Arg⁴³ (red), Asn¹¹⁰ (pink), His¹¹¹ (cyan), Leu¹⁹⁶ (blue), Phe²¹⁰ (magenta; in h7h8) and Cys²⁵³ (yellow). The model is based, as indicated in Materials and Methods, in the structure of the zebrafish homolog (PDB ID 2NXF).

doi:10.1371/journal.pone.0118680.g001

To simulate the binding of substrates to human ADPRibase-Mn, a homology model, based on the known structure of zebrafish ADPRibase-Mn, was taken from a public repository and completed as described under Materials and Methods. It displayed a deep pocket with a dinuclear center in the bottom and a metal-bridging water. Around the pocket entrance stood the unique regions s2s3, h2, and h7h8 (Fig. 1). ADP-ribose, cADPR, CDP-choline and 2',3'-cAMP were independently docked to this site (S4 Fig.).

The conformation of ADP-ribose docked to the model of human ADPRibase-Mn is shown in Fig. 2, which displays also the amino acids that interact with ADP-ribose as identified by analysis with VMD. This included amino acids belonging (i) to the ADPRibase-Mn-unique regions s2s3 (Phe³⁷ and Arg⁴³) or h7h8 (Phe²¹⁰), (ii) to the MDP superfamily motif (Gln²⁷, Asn¹¹⁰ and His¹¹¹), or (iii) to the short h10 helix (Cys²⁵³). These seven amino acids interact also with ADP-ribose docked to a homology model of rat ADPRibase-Mn [2]. Their locations in human ADPRibase-Mn are highlighted in Fig. 1, as it is the position of Leu¹⁹⁶ within h7h8 because, although it did not interact with ADP-ribose docked to human ADPRibase-Mn, it does so with the substrate docked to rat ADPRibase-Mn [2]. These eight amino acids of the human enzyme were subjected to mutagenesis.

Point mutations in human ADPRibase-Mn and effects on kinetic parameters

Most of the mutations implemented were intended to inactivate a potential effect of the interacting amino acid, and the native residues were changed to alanine (some control mutations

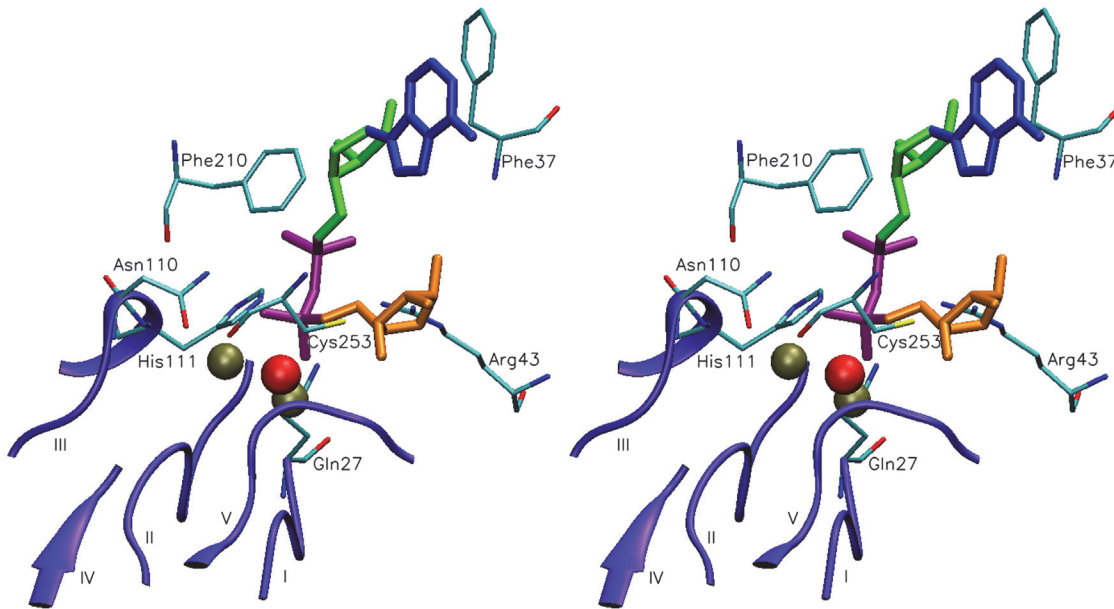


Fig 2. Stereogram of ADP-ribose docked to the active site of the model structure of human ADPRibase-Mn: identification of interacting amino acids. Besides ADP-ribose, the model shows the dimetallic center bound to the five short consensus regions of the MDP-superfamily motif (I-V, violet), and the amino acids identified by their interaction with docked ADP-ribose (see the main text for details). This set of hypothetical interactions was the starting point for the mutagenesis experiments. The conformation shown in the figure was the starting structure for the molecular dynamics simulation of the enzyme-substrate complex (Fig. 3).

doi:10.1371/journal.pone.0118680.g002

were performed to non-alanine residues). The only exception was the mutation of Gln²⁷, aimed to test the effects of its substitution by a histidine residue, which is present in other MDP proteins.

The effects of the mutations were tested by kinetic assay of k_{cat} , K_m and k_{cat}/K_m with ADP-ribose, CDP-choline, 2',3'-cAMP and cADPR. With the latter substrate, in many cases, rather than measuring k_{cat} and K_m from saturation curves, the catalytic efficiency parameter k_{cat}/K_m was directly estimated under conditions of rate linearity versus cADPR concentration, i.e. at cADPR concentrations well below the K_m value [4, 52, 56]. The results are summarized in Table 1.

The majority of the mutations to alanine of the amino acids interacting with ADP-ribose diminished the catalytic efficiency for this substrate to different extents. Sometimes, but not always, roughly similar decreases of efficiency were observed with the other substrates. However, an important exception was the absence of negative effect of mutating Cys²⁵³ which, as stated above, was the only residue unrelated to the disperse motif of the MDP superfamily and to the regions unique to the ADPRibase-Mn-like family. Actually, the C253A mutant displayed a ten-fold increased efficiency over cADPR, with no or modest effect on the other substrates. The meaning of these and other results of the mutagenesis study, which included a few double and one triple mutant, is presented and discussed below in detail.

Roles of amino acids belonging to the disperse motif of the MDP superfamily: Gln²⁷, Asn¹¹⁰ and His¹¹¹

Three of the amino acids that have been mutated in human ADPRibase-Mn belong to two of the short consensus regions of the MDP superfamily motif.

Gln²⁷ occupies the third position of the first consensus region (DX[H/X]), that in the ADPRibase-Mn-like family is conserved as D[V/I]Q with very few exceptions (see [S3 Fig.](#)). In the docking model with ADP-ribose, the carbonyl group of Gln²⁷ side chain is coordinated with one of the metal ions (metal 1), and the amide NH₂ is near to form a hydrogen bond with one of the oxygens of the β phosphate of ADP-ribose. We chose to implement the Q27H mutation that does not eliminate the possibility of side-chain interactions and converts the D[V/I]Q region to D[V/I]H that is the more general consensus of the MDP superfamily [[59–63](#)]. The mutation did not change the relative preference of the enzyme for the four substrates considered as it reduced to the same extent (≈11–13-fold reduction) the catalytic efficiency of the hydrolysis of ADP-ribose, CDP-choline or 2',3'-cAMP, and only somewhat more strongly (≈27-fold reduction) the hydrolysis of cADPR (see [Table 1](#)). However, the effects on k_{cat} and K_{m} differed among the three first substrates. The k_{cat} value diminished 4 fold for ADP-ribose, was unchanged for CDP-choline and diminished 14 fold for 2',3'-cAMP. The K_{m} value augmented 3 fold for ADP-ribose, 8 fold for CDP-choline and did not change for 2',3'-cAMP. There was no data available on k_{cat} and K_{m} for cADPR. In summary, for ADP-ribose, the Q27H substitution elicited modest negative effects of similar magnitude in catalysis and in substrate binding. For CDP-choline, the substitution did not affect catalysis, only binding. On the contrary, for 2',3'-cAMP, the substitution affected catalysis not binding, perhaps because the larger size of histidine made less likely for this substrate to adopt a favorable orientation of the scissile P-O bond with respect to the water nucleophile.

Asn¹¹⁰ is part of the GNH[D/E] consensus region as an invariant residue ([S3 Fig.](#)). In the docking model with ADP-ribose, the side-chain carbonyl of Asn¹¹⁰ is coordinated with one of the metal ions (metal 2) and its amide NH₂ is donor in a hydrogen bond with one of the oxygens of the phosphate of ADP-ribose. We chose to implement in this case a N110A mutation that might affect both the coordination sphere of the dinuclear center and the binding of substrate. The effects of this substitution on kinetic parameters ([Table 1](#)) showed a complex response that partly recalled the effects of the Q27H mutation but with a few important differences. First, with the N110A substitution the reduction of catalytic efficiency was stronger (100–250 fold) for the hydrolysis of CDP-choline or 2',3'-cAMP than for the hydrolysis of ADP-ribose or cADPR (30–40 fold). The decrease of k_{cat} value was stronger for the hydrolysis of 2',3'-cAMP which was 550 fold smaller than the wild type k_{cat} . The changes of K_{m} were little different to those elicited by the Q27H substitution. The results of this mutation are difficult to interpret as, besides the possible effects on the metal coordination sphere and on the binding of substrate, the proximity of Asn¹¹⁰ to His¹¹¹ could affect the interaction of the latter with substrates (see below).

His¹¹¹ is also an invariant residue of the GNH[D/E] consensus like Asn¹¹⁰ ([S3 Fig.](#)), and in non-ADPRibase-Mn MDPs it has been found important in catalysis but not involved in metal coordination [[78–81](#)]. In ADPRibase-Mn, the GNH[D/E] histidine residue is neither involved in metal coordination, but is at hydrogen bond distance of the phosphoanhydride oxygen of diphosphate substrates or of the 2'-phosphoester of 2',3'-cAMP ([S4 Fig.](#)). This has been observed also in docking complexes of zebrafish ADPRibase-Mn [[52](#)]. We implemented two His¹¹¹ mutants: H111A and H111N. The first one caused a marked efficiency decrease with all substrates except 2',3'-cAMP, which was little affected. The same response pattern was produced by the equivalent mutation in zebrafish ADPRibase-Mn [[52](#)]. These results support the previously suggested role of this histidine residue in catalysis through an orientation effect augmenting the probability of a near in-line attack of the metal-bridging water over the P-O scissile bond [[52](#), [80](#)]. The action of the GNH[D/E] histidine of ADPRibase-Mn as a general acid catalyst seems unlikely in view of the modest or null effect of the mutation on the kinetic parameters of the hydrolysis of the 2',3'-cAMP phosphodiester, as opposed to the strong effect

on the hydrolysis of the phosphoanhydride linkage of the other substrates (Table 1, and [52]). The importance of general acid catalysis should be, if something, more obvious for the hydrolysis of a phosphodiester than a phosphoanhydride, as the former would profit from a proton donor to yield an alcohol leaving group. A similar reasoning can be made from the results of the H111N mutation, as being the asparagine side chain unable to act as general catalyst, the results of this substitution did neither affect the kinetic parameters of 2',3'-cAMP phosphodiester hydrolysis. On the other hand, concerning the possible orientation effect, the (near) independence of 2',3'-cAMP hydrolysis on the GNH[D/E] histidine would be explainable by the structural rigidity of this substrate and its straightforward fit in the active site with the in-line orientation [52].

The unique structural element s2s3 in human ADPRibase-Mn: catalytic role of Arg⁴³ and role of Phe³⁷ in the enzyme preference for ADP-ribose

In the human ADPRibase-Mn, the unique region s2s3 is formed by amino acids 30–45 (S5 Fig.). From the mutagenesis experiments, the two s2s3 amino acids that interacted with ADP-ribose, Arg⁴³ and Phe³⁷, emerged as critically relevant to the catalytic mechanism or the specificity.

The sidechain of Arg⁴³ points towards the pyrophosphate groups of ADP-ribose (Fig. 2) and probably of the other docked substrates (S4 Fig.). This residue is invariant in the ADPRibase-Mn-like family (S3 Fig.), and it could have a role in stabilizing the transition state and/or the leaving group. In agreement with this catalytic role, the R43A mutant showed a drastic, four-orders-of-magnitude decrease of catalytic efficiency (k_{cat}/K_m) with all the substrates except 2',3'-cAMP, for which only a 200-fold decrease of efficiency was observed (Table 1). This, though quite strong an effect, indicates, together with the modest or null effects of His¹¹¹ mutations, that the catalytic requirements for the hydrolysis of 2',3'-cAMP by human ADPRibase-Mn are lesser than for the other substrates (see above: Table 1 and [52]).

In the hypothetical conformation adopted by ADP-ribose in the docking model, the hydrophobic ring of Phe³⁷ made a contact with the nitrogenous base, which was not observed with the other docked substrates (S4 Fig.). Since the ADPRibase-Mn preference for ADP-ribose was characterized by a considerably lower K_m when compared to the other substrates (Table 1), the potential specificity of the interaction with Phe³⁷ suggested that this amino acid could be a determinant for the ADP-ribose preference. In agreement with this view, the F37A mutant displayed a 19-fold increased K_m for ADP-ribose, with only a 2–3-fold increase of the CDP-choline and 2',3'-cAMP K_m values. At the same time only minor decreases of k_{cat} were elicited by the same mutation. In terms of k_{cat}/K_m , the F37A mutation diminished the efficiency of ADP-ribose hydrolysis by 50 fold, but that of the other substrates, including cADPR, was reduced by only 3–4 fold. The control mutant F37Y showed the same kinetic parameters as the wild type. In summary, the preferred substrate of F37A-ADPRibase-Mn was CDP-choline, indicating that the preference of wild type ADPRibase-Mn by ADP-ribose is determined by Phe³⁷. This residue is widely conserved as phenylalanine or tyrosine, in animals and plants with some substitutions by aliphatic amino acids in protist ADPRibase-Mn proteins (S3 Fig.). It would be interesting to learn the natural specificity of proteins of this family having Phe³⁷ replaced by a nonaromatic residue.

Additional support for the interaction of ADP-ribose with Phe³⁷ within s2s3 came from simulations of molecular dynamics (see below).

Effects of docked ADP-ribose on the simulated molecular dynamics of the ADPRibase-Mn model

To search for possible effects of the binding of ADP-ribose to the active site of human ADPRibase-Mn, 40-ns simulations of molecular dynamics of the ADPRibase-Mn:ADP-ribose model obtained by docking, and of the free enzyme, were run and compared (Fig. 3). In the dynamic trajectory, four protein regions showed a substrate-dependent decrease of mobility, one of them apparently related to the proximity of bound ADP-ribose. The mobility of the backbone C atoms was quantitated by measuring their root mean square fluctuations (RMSF) along the trajectories, which identified the regions of diminished mobility as those formed by amino acids 7–14, 34–41, 78–84 and 333–342. The first and the last of those regions correspond to the polypeptide ends. Interestingly, region 34–41 is included in s2s3 (amino acids 30–45) and region 78–84 coincides well with h2 (amino acids 78–85), which have been identified as regions unique to the ADPRibase-Mn-like family (Fig. 1, S5 Fig. and [52]). On the other hand, region h7h8 (amino acids 170–212), also unique to this family, showed high mobility in its central part (amino acids 175–205) but was little affected by the presence of bound ADP-ribose in the simulation (Fig. 3).

In summary, the decreased mobility of the s2s3 element (which contains the ADP-ribose-specificity determinant Phe³⁷) in the presence of docked ADP-ribose, supports the importance of the interaction of the substrate with the amino acid.

The unique structural element h7h8 in human ADPRibase-Mn: relevance of Leu¹⁹⁶ and Phe²¹⁰

The unique structural element h7h8 of human ADPRibase-Mn is formed by amino acids 170–212 (S5 Fig.). Within it, we focused on Leu¹⁹⁶ and Phe²¹⁰. To judge from single-point mutations, only the latter had a clearcut repercussion over enzyme action. However, some relevance of Leu¹⁹⁶ was inferred from the analysis of double mutants.

Leu¹⁹⁶ is conserved in vertebrates but not in most of the ADPRibase-Mn proteins belonging to other taxa (S3 Fig.). This amino acid is located approximately opposite the specificity determinant Phe³⁷, not very far from it across the entrance to the active site (Fig. 1). Together, these two amino acids could favor a closed conformation of the active site. In a docking model of ADP-ribose with rat ADPRibase-Mn, Leu¹⁹⁶ is close to the adenine ring [2], but a similar contact was not seen in the docking complex with the modeled human enzyme (Fig. 2). However, mutagenesis of Leu¹⁹⁶ had interesting if subtle effects. The L196A point mutation caused only a modest 2–5-fold decrease of catalytic efficiency with the four substrates tested. The F37A+L196A double mutant showed a modest enhancement of the inhibitory effect over that of the F37A point mutation. Unexpectedly, such effect was even slightly stronger with the control double mutation F37A+L196F, except for the activity on cADPR, which was less affected than by F37A+L196A (Table 1). The effect of Leu¹⁹⁶ mutagenesis is best illustrated by the ratio of catalytic efficiencies ADP-ribose/cADPR: 150 for the wild type; 9.2 for F37A; 6.7 for F37A+L196A; 3.0 for F37A+L196F. The minor effect of the Leu¹⁹⁶ substitutions, that favored the cADPR phosphohydrolase activity in relative terms, was taken to advantage, in a synergistic combination with the C253A mutation, to obtain an ADPRibase-Mn triple mutant that displayed preferential activity on cADPR (see below).

The sidechain of Phe²¹⁰, which is widely conserved in the ADPRibase-Mn family (S3 Fig.), lays beside the substrate, near the pyrophosphate and the two riboses in the docking model with ADP-ribose, acting perhaps as a stanchion that keeps the substrate into position (Fig. 2). Its relevance was supported by the effects of the F210A mutation, which lowered 40–70 fold the catalytic efficiency for ADP-ribose, CDP-choline and 2',3'-cAMP hydrolysis, and 500 fold

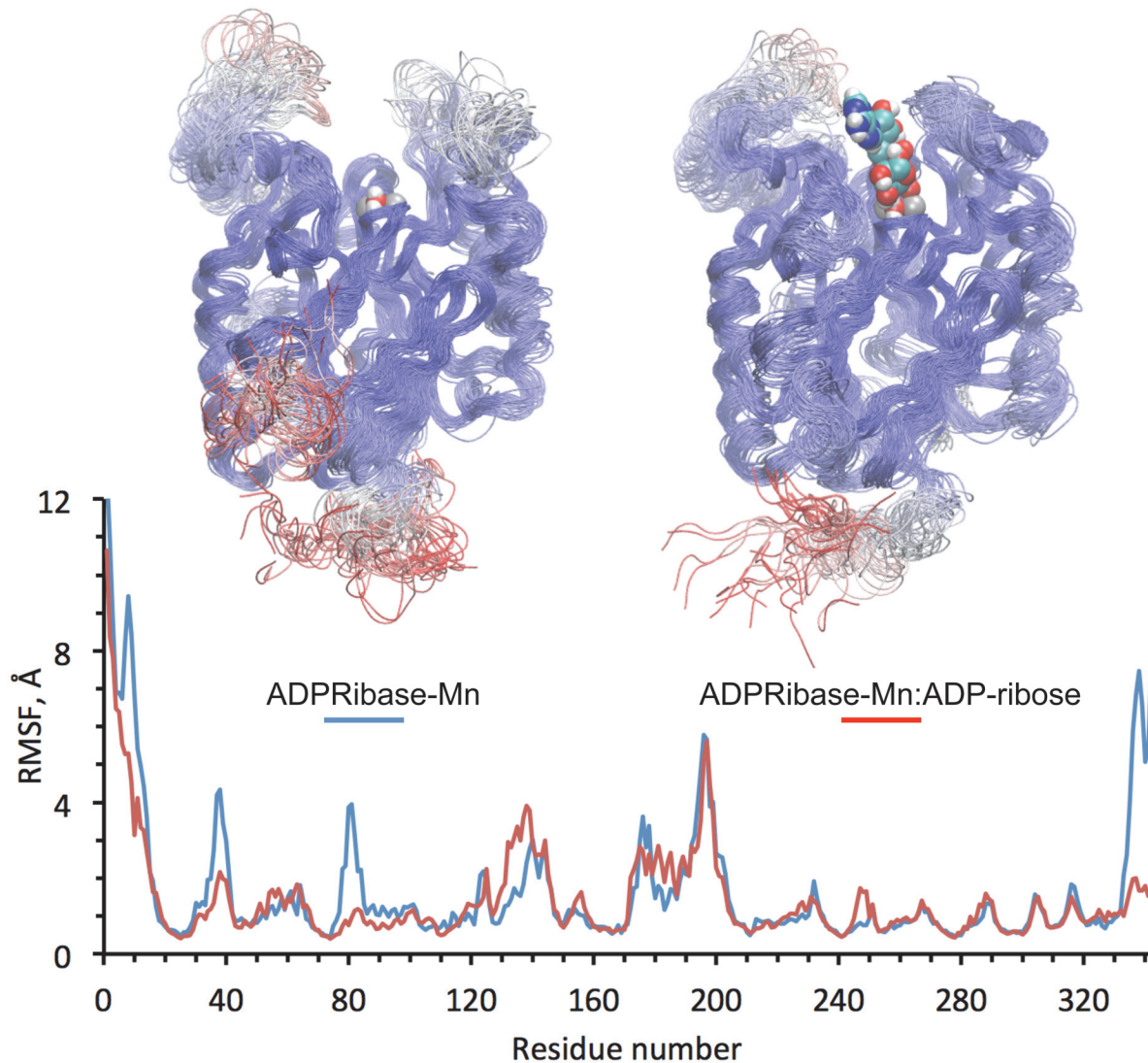


Fig 3. Molecular dynamics simulation of the complex of modeled human ADPRibase-Mn with ADP-ribose, and its comparison to the substrate-free enzyme. Simulations of 40 ns were implemented as described under Materials and Methods. The upper protein models show the overlap of 40 snapshots taken at 1-ns intervals, with the protein backbone represented as a thin tube colored by mobility (red, maximal mobility; blue minimal mobility). The left-hand side and the right-hand side models contain the dimetallic center and the bridging water, and the right-hand side one contains also docked ADP-ribose colored by element. These ligands are shown in the positions occupied at the beginning of the simulations. The lower graph shows the mobility of the C α atoms of the protein backbone quantitated as RMSF values.

doi:10.1371/journal.pone.0118680.g003

for cADPR (Table 1). The decrease of k_{cat}/K_m was due to increases of K_m for ADP-ribose and CDP-choline, with little effect on k_{cat} values, but mainly to a decrease of k_{cat} for 2',3'-cAMP. The different response of the latter to the F210A mutation could be related to the rigidity of 2',3'-cAMP and to a lower probability of adopting a conformation with the scissile P-O bond in line with the water nucleophile in the absence of the phenyl group of Phe²¹⁰. The more flexible structures of ADP-ribose and CDP-choline, though binding with lower affinities in the absence of the aromatic ring of Phe²¹⁰, would then be as likely to adopt the conformation favorable to the nucleophilic attack as when bound to the wild-type enzyme.

Role of Cys²⁵³ as a factor limiting the cADPR phosphohydrolase activity of ADPRibase-Mn

Most of the mutations tested either diminished the catalytic efficiency of cADPR phosphohydrolase or elicited only modest changes, more or less in parallel to changes of efficiency on the other substrates considered (Table 1). Anyhow, there were two important exceptions to this general trend. One was observed in the effects of the F37A mutation which, as discussed below, revealed Phe³⁷ is a major determinant of the preference of ADPRibase-Mn for ADP-ribose as substrate, with a comparatively minor effect on the hydrolysis of the other substrates, cADPR included. The other exception, more relevant to the character of the cADPR phosphohydrolase activity, was the effect of the C253A mutation, which unexpectedly elicited a specific increase (10 fold) of the catalytic efficiency over cADPR, composed by a decrease of the K_m (to a value similar to those of the rat and the zebrafish enzymes), and an increase of k_{cat} . In comparison, the removal of the thiol group of Cys²⁵³ did not affect or caused a very slight increase of the apparent affinity of the enzyme for the other substrates. It seems that this residue hinders the optimal binding of cADPR to the active site of human ADPRibase-Mn.

Cys²⁵³ is extensively conserved among vertebrates, but not in ADPRibase-Mn-like proteins of other taxa in which the family is present (S3 Fig.). Whether non-vertebrate enzymes, particularly those of higher plant origin in which alanine occupies naturally the position equivalent to human Cys²⁵³, could be better cADPR phosphohydrolase catalysts than mammalian ADPRibase-Mn remains speculative.

Construction of a triple mutant preferentially active on cADPR

As a proof of principle that the specificity for cADPR can be augmented by mutagenesis, the triple ADPRibase-Mn mutant F37A+L196F+C253A was constructed. In it, the double mutation F37A+L196F, which had been shown to lessen the relative preference for ADP-ribose *versus* cADPR, was combined with the specific activation of cADPR phosphohydrolase produced by the C253A mutation in absolute terms. Had this combination produced additive effects, one would expect that the resulting protein displayed a ratio of catalytic efficiencies cADPR/ADP-ribose about 2. In fact, the kinetic characterization of the triple mutant gave a k_{cat}/K_m value of $35500 \text{ M}^{-1}\text{s}^{-1}$, 3.2-fold higher than the efficiency of ADP-ribose hydrolysis, and also higher than those of CDP-choline and 2',3'-cAMP (Table 1). The k_{cat}/K_m values for other ADPRibase-Mn substrates not included in the kinetic study of mutants were also assayed with the triple mutant to proof that they were also lower than with cADPR, namely CDP-glycerol, $22000 \pm 4000 \text{ M}^{-1}\text{s}^{-1}$; CDP-ethanolamine, $5800 \pm 700 \text{ M}^{-1}\text{s}^{-1}$; ADP, $53 \pm 12 \text{ M}^{-1}\text{s}^{-1}$.

Concluding discussion

First, we would like to emphasize that the structural and dynamic information on human ADPRibase-Mn presented in this study comes from homology modeling and simulation studies of docking and molecular dynamics. The strength of this approach is not comparable to what NMR or X-ray studies of actual structures and interactions would afford. In particular, one has to be aware that the docking itself produces speculative information and may give false positives. Therefore, data relative to interactions, positions, angles or distances measured on the human ADPRibase-Mn models should be taken as hypothetical. We have used these data as starting point to choose residues for mutation, and as arguments to help in the interpretation of the kinetic behavior of mutant proteins.

The dinuclear center of the crystal structure of zebrafish ADPRibase-Mn contains a metal-bridging molecule of water that was included in the homology model of the human enzyme to

which the substrates were docked. Based mainly on the docking of ADP-ribose to this model, eight amino acids of human ADPRibase-Mn were selected for mutagenesis. To analyze the results of the mutagenesis and enzyme kinetics studies, it was hypothesized that the bridging metal-activated water or hydroxide could be the attacking nucleophile like in the mechanisms of other phosphoesterases [61, 69]. According to this model, substrates need correct positioning in the active center for the attack to be made under near in-line conditions. Another mechanistic aspect here considered is the possible stabilization of the transition state of the reactions by charge neutralization.

Several ADPRibase-Mn amino acids with roles in catalysis and/or substrate specificity have been identified in this study. In many cases, the kinetic effects of a particular mutation were different depending on the substrate considered. A corollary of this picture is that the correct positioning of each substrate may depend, more or less strictly, on a different set of amino acids. Not surprisingly, substrate-positioning residues may have bearing both on catalysis (k_{cat}) and substrate binding (K_{m}).

Two amino acids appeared clearly involved in catalysis. (i) Arg⁴³, due to the proximity of its sidechain end to the substrate phosphoryl group(s), probably stabilizes the transition state and/or the leaving group by charge neutralization. Comparing the hydrolytic reactions with different substrates, the bearing of Arg⁴³ on catalysis was less dramatic (but quite strong at any rate) for the hydrolysis of 2',3'-cAMP, perhaps because of the single phosphoryl group, and the relatively low activation energy of hydrolysis of its P-O2' ester linkage [82]. (ii) His¹¹¹, that may form a hydrogen bond with the O atom of the scissile P-O bond, probably helps to keep the substrate in a position susceptible of in-line nucleophilic attack by the metal-activated water. Again, the bearing of His¹¹¹ on catalysis was less marked with 2',3'-cAMP as the substrate. As a consequence, this was the best substrate for the H111A-ADPRibase-Mn mutant. A similar effect of the equivalent residue and mutation, observed with zebrafish ADPRibase-Mn, has been attributed to the low conformational flexibility of this compound and to its lesser need of assisted orientation towards the in-line position [52]. Another substrate-specific effect of His¹¹¹ concerned substrate binding, since its mutation increased the K_{m} for CDP-choline, but not for the other substrates.

Another two residues appeared clearly involved in substrate specificity. (i) Phe³⁷ is located in the rim of the entrance to the active site, distant from the catalytic core around the dinuclear center. In such position, Phe³⁷ acts as the determinant of the ADPRibase-Mn preference for ADP-ribose, possibly due to a specific interaction of the aromatic residue with the nitrogenous base of ADP-ribose. The other substrates do not seem to make this contact in their docking models. The larger observed effect of the F37A mutation was the increase of the K_{m} for ADP-ribose, with only modest effects on the k_{cat} values or on the K_{m} s for CDP-choline and 2',3'-cAMP. Therefore, the best substrate of the F37A mutant was no longer ADP-ribose, but CDP-choline. (ii) Cys²⁵³ is located near the catalytic core and the dinuclear center, without evidence for interaction with the metals. The SH group is at near contact distance with the C3 of the non-nucleosidic ribose of ADP-ribose or the "northern" ribose of cADPR. Interestingly, this does not seem to be a favorable contact, but a subtle obstacle to optimal cADPR binding and positioning, thus limiting the phosphohydrolytic activity on this substrate. The C253A mutation elicited modest but favorable effects both in k_{cat} and K_{m} for cADPR, what brought about a significant and unique increase in catalytic efficiency on this substrate. This was the only point mutation bringing about an efficiency increase. Two other mutations together (F37A and L196A), although eliciting negative effects in absolute terms, affected less the hydrolysis of cADPR than of other substrates. The result of combining the three mutations (F37A+L196F+C253A) was an ADPRibase-Mn protein that acted preferentially as cADPR phosphohydrolase.

In summary, this work sheds light on the mechanism and specificity of human ADPRibase-Mn and paves the way for identifying more specific cADPR phosphohydrolases, perhaps among ADPRibase-Mn-like proteins in which Cys²⁵³ is not conserved, and/or for designing ADPRibase-Mn mutants with such specificity. This future goal could be compared to the reported conversion of CD38 by mutagenesis from a predominant NAD glycohydrolase to a specific ADP-ribosyl cyclase [83]. A specific cADPR phosphohydrolase would make a useful tool for in vitro analytical and in vivo functional studies of this regulator.

Supporting Information

S1 Dataset. Coordinates of the docking complex of the model structure of human ADPRibase-Mn with ADP-ribose.

(PDB)

S2 Dataset. Coordinates of the docking complex of the model structure of human ADPRibase-Mn with cADPR.

(PDB)

S3 Dataset. Coordinates of the docking complex of the model structure of human ADPRibase-Mn with CDP-choline.

(PDB)

S4 Dataset. Coordinates of the docking complex of the model structure of human ADPRibase-Mn with 2',3'-cAMP.

(PDB)

S1 Fig. pH requirements of human ADPRibase-Mn activities. The assays were performed with 500 μ M substrate in the presence of 5 mM MnCl₂ at the indicated pH values using 100 mM Tris/acetate (pH 6.03 and 6.67), 100 mM Tris/HCl (pH 6.55, 7.08, 7.46, 7.73, 8.29, 8.55, 8.94 and 9.68) or 100 mM glycine/NaOH (8.89, 9.93 and 10.50). The pH values were measured with a glass electrode in reaction mixtures at the assay temperature of 37°C. The results are means with S.D. of three experiments.

(PDF)

S2 Fig. Mn²⁺ requirements of human ADPRibase-Mn activities. In this experiment the means \pm S.D. were obtained in triplicate assays performed at pH 7.5, with 500 μ M ADP-ribose or CDP-choline, or with 2500 μ M 2',3'-cAMP, in the presence of the indicated MnCl₂ concentrations. The response of activity to Mn²⁺ concentration (5 μ M-5000 μ M) is representative of several other experiments performed under different experimental conditions.

(PDF)

S3 Fig. Sequence alignment of 108 eukaryotic proteins representative of the ADPRibase-Mn-like family. The names of species and GenBank accession numbers of the proteins are colored according to the following code: *black*, vertebrates; *blue*, invertebrate animals; *red*, plants; *orange*, protists. All the proteins were sorted out from a BlastP search [57] run on July 7, 2014. The proteins shown were selected applying criteria described under Materials and Methods, except for the selection of a few additional proteins: (i) the one from *Mus musculus*, despite being 96% identical to that from *Rattus norvegicus*, and due to its classification as the product of an immune gene [2, 37]; (ii) those from *Bos taurus* and *Ovis aries*, despite being 97% identical, because these species are included in NCBI RefSeq Genomes; (iii) those from the bivalve *Crassostrea gigas*, the snail *Lottia gigantea*, and the worm *Helobdella robusta*, despite not being yet recorded in NCBI_RefSeq, due to their importance as possible representatives of the protein

family in invertebrate animal phyla. Residues identically conserved in all sequences are denoted by white letters on red background. Other regions of high sequence conservation are indicated by boxed red letters on white background. The numbers above the sequences correspond to the human protein. *Blue triangles* mark the amino acids that were mutated in this study. *Red rectangles* mark the five short regions that together form the disperse amino acid motif of the MDP superfamily. The unique regions s2s3, h2 and h7h8, typical of the ADPRibase-Mn family [52], are also indicated above the human protein.

(PDF)

S4 Fig. Stereograms of substrates docked to the active site of the model structure of human ADPRibase-Mn. The views show metals, metal-bridging water, and amino acids identified by their interaction with docked ADP-ribose and tested by mutagenesis (see the main text for details). The models illustrate the hypothesis that the metal bridging water, according to its location, could be the attacking nucleophile in the ADPRibase-Mn reactions. The nucleophilic attack distances are drawn only to emphasize this hypothesis.

(PDF)

S5 Fig. Topology diagram of the model structure of human ADPRibase-Mn. Structural elements (triangle, strand; circles, helix) are shown according to their numbering (strands 1–15 and helices 1–12) in zebrafish ADPRibase-Mn [52]. All the other numbers identify residues of human ADPRibase-Mn. The small golden circles are the metals of the dinuclear center; the eight amino acids of human ADPRibase-Mn coordinated to the metals are indicated. Strand 6 and helix 8 are present in the zebrafish protein; however, in the human protein, strand 6 is just a beta bridge and helix 8 was missing in the model downloaded from SWISS-MODEL to prepare the complete model structure of human ADPRibase-Mn (see [Materials and Methods](#) and [Fig. 1](#)), but appears in more recent models in the same repository [53].

(PDF)

S1 Table. Forward primers used for site-directed mutagenesis. The reverse primers were the reverse complements of those shown.

(PDF)

S2 Table. Purity of the recombinant protein preparations. In each case, enzyme purity was estimated by Coomassie blue-stained SDS-PAGE followed by image analysis quantitation.

(PDF)

S3 Table. Substrate specificity of human ADPRibase-Mn. The activities were assayed in triplicate with 500 μ M substrate in the presence of 5 mM MnCl_2 . The results are mean values with S.D. The sensitivity limit of the assay is indicated when no activity was detected.

(PDF)

Acknowledgments

We are grateful to Antonio Sillero and María Antonia Günther Sillero (Departamento de Bioquímica, Facultad de Medicina e Instituto de Investigaciones Biomédicas Alberto Sols, Universidad Autónoma de Madrid/Consejo Superior de Investigaciones Científicas, Madrid, Spain) for being an invaluable source of inspiration and gifts.

Author Contributions

Conceived and designed the experiments: AC AF JC JCC JMR JRR MJC RMP. Performed the experiments: AC AF ILV JC MJC RMP. Analyzed the data: JCC JMR JRR MJC. Wrote the paper: JCC JMR JRR. Run bioinformatics and molecular modeling: JMR JRR.

References

1. Canales J, Pinto RM, Costas MJ, Hernández MT, Miró A, Bernet D, et al. Rat liver nucleoside diphosphosugar or diphosphoalcohol pyrophosphatases different from nucleotide pyrophosphatase or phosphodiesterase I: substrate specificities of Mg²⁺- and/or Mn²⁺-dependent hydrolases acting on ADP-ribose. *Biochim Biophys Acta*. 1995; 1246: 167–177. PMID: [7819284](#)
2. Canales J, Fernández A, Ribeiro JM, Cabezas A, Rodrigues JR, Cameselle JC, et al. Mn²⁺-dependent ADP-ribose/CDP-alcohol pyrophosphatase: a novel metallophosphoesterase family preferentially expressed in rodent immune cells. *Biochem J*. 2008; 413: 103–113. doi: [10.1042/BJ20071471](#) PMID: [18352857](#)
3. Ash DE, Schramm VL. Determination of free and bound manganese(II) in hepatocytes from fed and fasted rats. *J Biol Chem*. 1982; 257: 9261–9264. PMID: [6286611](#)
4. Canales J, Fernández A, Rodrigues JR, Ferreira R, Ribeiro JM, Cabezas A, et al. Hydrolysis of the phosphoanhydride linkage of cyclic ADP-ribose by the Mn²⁺-dependent ADP-ribose/CDP-alcohol pyrophosphatase. *FEBS Lett*. 2009; 583: 1593–1598. doi: [10.1016/j.febslet.2009.04.023](#) PMID: [19379742](#)
5. Kuhn FJ, Luckhoff A. Sites of the NUDT9-H domain critical for ADP-ribose activation of the cation channel TRPM2. *J Biol Chem*. 2004; 279: 46431–46437. PMID: [15347676](#)
6. Kolisek M, Beck A, Fleig A, Penner R. Cyclic ADP-ribose and hydrogen peroxide synergize with ADP-ribose in the activation of TRPM2 channels. *Mol Cell*. 2005; 18: 61–69. PMID: [15808509](#)
7. Perraud AL, Takanishi CL, Shen B, Kang S, Smith MK, Schmitz C, et al. Accumulation of free ADP-ribose from mitochondria mediates oxidative stress-induced gating of TRPM2 cation channels. *J Biol Chem*. 2005; 280: 6138–6148. PMID: [15561722](#)
8. Gasser A, Glassmeier G, Flieger R, Langhorst MF, Meinke S, Hein D, et al. Activation of T cell calcium influx by the second messenger ADP-ribose. *J Biol Chem*. 2006; 281: 2489–2496. PMID: [16316998](#)
9. Yu P, Wang Q, Zhang LH, Lee HC, Zhang L, Yue J. A cell permeable NPE caged ADP-ribose for studying TRPM2. *PLoS One*. 2012; 7: e51028. doi: [10.1371/journal.pone.0051028](#) PMID: [23236422](#)
10. Clementi E, Riccio M, Sciorati C, Nistico G, Meldolesi J. The type 2 ryanodine receptor of neurosecretory PC12 cells is activated by cyclic ADP-ribose. Role of the nitric oxide/cGMP pathway. *J Biol Chem*. 1996; 271: 17739–17745. PMID: [8663443](#)
11. Ogunbayo OA, Zhu Y, Rossi D, Sorrentino V, Ma J, Zhu MX, et al. Cyclic adenosine diphosphate ribose activates ryanodine receptors, whereas NAADP activates two-pore domain channels. *J Biol Chem*. 2011; 286: 9136–9140. doi: [10.1074/jbc.M110.202002](#) PMID: [21216967](#)
12. Lee HC. Cyclic ADP-ribose and nicotinic acid adenine dinucleotide phosphate (NAADP) as messengers for calcium mobilization. *J Biol Chem*. 2012; 287: 31633–31640. doi: [10.1074/jbc.R112.349464](#) PMID: [22822066](#)
13. Ferrero E, Lo Buono N, Horenstein AL, Funaro A, Malavasi F. The ADP-ribosyl cyclases—the current evolutionary state of the ARCs. *Front Biosci*. 2014; 19: 986–1002. PMID: [24896331](#)
14. Lee HC, Aarhus R. ADP-ribosyl cyclase: an enzyme that cyclizes NAD⁺ into a calcium-mobilizing metabolite. *Cell Regul*. 1991; 2: 203–209. PMID: [1830494](#)
15. Inageda K, Takahashi K, Tokita K, Nishina H, Kanaho Y, Kukimoto I, et al. Enzyme properties of *Aplysia* ADP-ribosyl cyclase: comparison with NAD glycohydrolase of CD38 antigen. *J Biochem*. 1995; 117: 125–131. PMID: [7775378](#)
16. Liu Q, Graeff R, Kriksunov IA, Jiang H, Zhang B, Oppenheimer N, et al. Structural basis for enzymatic evolution from a dedicated ADP-ribosyl cyclase to a multifunctional NAD hydrolase. *J Biol Chem*. 2009; 284: 27637–27645. doi: [10.1074/jbc.M109.031005](#) PMID: [19640846](#)
17. Takasawa S, Tohgo A, Noguchi N, Koguma T, Nata K, Sugimoto T, et al. Synthesis and hydrolysis of cyclic ADP-ribose by human leukocyte antigen CD38 and inhibition of the hydrolysis by ATP. *J Biol Chem*. 1993; 268: 26052–26054. PMID: [8253715](#)
18. Kim H, Jacobson EL, Jacobson MK. Synthesis and degradation of cyclic ADP-ribose by NAD glycohydrolases. *Science*. 1993; 261: 1330–1333. PMID: [8395705](#)
19. Howard M, Grimaldi JC, Bazan JF, Lund FE, Santos-Argumedo L, Parkhouse RM, et al. Formation and hydrolysis of cyclic ADP-ribose catalyzed by lymphocyte antigen CD38. *Science*. 1993; 262: 1056–1059. PMID: [8235624](#)

20. Zocchi E, Franco L, Guida L, Benatti U, Bargellesi A, Malavasi F, et al. A single protein immunologically identified as CD38 displays NAD⁺ glycohydrolase, ADP-ribosyl cyclase and cyclic ADP-ribose hydrolyase activities at the outer surface of human erythrocytes. *Biochem Biophys Res Commun*. 1993; 196: 1459–1465. PMID: [8250903](#)
21. Hirata Y, Kimura N, Sato K, Ohsugi Y, Takasawa S, Okamoto H, et al. ADP ribosyl cyclase activity of a novel bone marrow stromal cell surface molecule, BST-1. *FEBS Lett*. 1994; 356: 244–248. PMID: [7805847](#)
22. Berthelie V, Tixier JM, Muller-Steffner H, Schuber F, Deterre P. Human CD38 is an authentic NAD(P)⁺ glycohydrolase. *Biochem J*. 1998; 330: 1383–1390. PMID: [9494110](#)
23. Liu Q, Kriksunov IA, Graeff R, Lee HC, Hao Q. Structural basis for formation and hydrolysis of the calcium messenger cyclic ADP-ribose by human CD38. *J Biol Chem*. 2007; 282: 5853–5861. PMID: [17182614](#)
24. Egea PF, Muller-Steffner H, Kuhn I, Cakir-Kiefer C, Oppenheimer NJ, Stroud RM, et al. Insights into the mechanism of bovine CD38/NAD⁺ glycohydrolase from the X-ray structures of its Michaelis complex and covalently-trapped intermediates. *PLoS One*. 2012; 7: e34918. doi: [10.1371/journal.pone.0034918](#) PMID: [22529956](#)
25. Gu Q-M, Sih CJ. Cyclic ADP-ribose: synthesis and structural assignment. *J Am Chem Soc*. 1994; 116: 7481–7486.
26. Khorana HG. Phosphodiesterases. In: Boyer PD, Lardy HA, Myrbäck K, editors. *The Enzymes*, 2nd ed, Vol 5. New York: Academic Press; 1961. p. 79–94.
27. Razzell WE. Phosphodiesterases. *Methods Enzymol*. 1963; 6: 236–258.
28. García-Díaz M, Ávalos M, Cameselle JC. Alcohol esterification reactions and mechanisms of snake venom 5'-nucleotide phosphodiesterase. *Eur J Biochem*. 1993; 213: 1139–1148. PMID: [8389294](#)
29. Sana TR, Gordon DB, Fischer SM, Tichy SE, Kitagawa N, Lai C, et al. Global mass spectrometry based metabolomics profiling of erythrocytes infected with *Plasmodium falciparum*. *PLoS One*. 2013; 8: e60840. doi: [10.1371/journal.pone.0060840](#) PMID: [23593322](#)
30. Guse AH, Cakir-Kiefer C, Fukuoka M, Shuto S, Weber K, Bailey VC, et al. Novel hydrolysis-resistant analogues of cyclic ADP-ribose: modification of the “northern” ribose and calcium release activity. *Biochemistry*. 2002; 41: 6744–6751. PMID: [12022878](#)
31. Guse AH. Biochemistry, biology, and pharmacology of cyclic adenosine diphosphoribose (cADPR). *Curr Med Chem*. 2004; 11: 847–855. PMID: [15078169](#)
32. Shuto S, Matsuda A. Chemistry of cyclic ADP-ribose and its analogs. *Curr Med Chem*. 2004; 11: 827–845. PMID: [15078168](#)
33. Moreau C, Liu Q, Graeff R, Wagner GK, Thomas MP, Swarbrick JM, et al. CD38 structure-based inhibitor design using the 1-cyclic inosine 5'-diphosphate ribose template. *PLoS One*. 2013; 8: e66247. PMID: [23840430](#)
34. Huang X, Dong M, Liu J, Zhang K, Yang Z, Zhang L, et al. Concise syntheses of trifluoromethylated cyclic and acyclic analogues of cADPR. *Molecules*. 2010; 15: 8689–8701. doi: [10.3390/molecules15128689](#) PMID: [21119564](#)
35. Wu H, Yang Z, Zhang L, Zhang L. Concise synthesis of novel acyclic analogues of cADPR with an ether chain as the northern moiety. *New J Chem*. 2010; 34: 956–966.
36. Swarbrick JM, Graeff R, Garnham C, Thomas MP, Galione A, Potter BV. ‘Click cyclic ADP-ribose’: a neutral second messenger mimic. *Chem Commun (Camb)*. 2014; 50: 2458–2461. doi: [10.1039/c3cc49249d](#) PMID: [24452494](#)
37. Hutton JJ, Jegga AG, Kong S, Gupta A, Ebert C, Williams S, et al. Microarray and comparative genomics-based identification of genes and gene regulatory regions of the mouse immune system. *BMC Genomics*. 2004; 5: 82. PMID: [15504237](#)
38. Malavasi F, Deaglio S, Ferrero E, Funaro A, Sancho J, Ausiello CM, et al. CD38 and CD157 as receptors of the immune system: a bridge between innate and adaptive immunity. *Mol Med*. 2006; 12: 334–341. PMID: [17380201](#)
39. Partida-Sánchez S, Rivero-Nava L, Shi G, Lund FE. CD38: an ecto-enzyme at the crossroads of innate and adaptive immune responses. *Adv Exp Med Biol*. 2007; 590: 171–183. PMID: [17191385](#)
40. Postigo J, Iglesias M, Cerezo-Wallis D, Rosal-Vela A, Garcia-Rodríguez S, Zubiaur M, et al. Mice deficient in CD38 develop an attenuated form of collagen type II-induced arthritis. *PLoS One*. 2012; 7: e33534. doi: [10.1371/journal.pone.0033534](#) PMID: [22438945](#)
41. Ernst IM, Fliegert R, Guse AH. Adenine dinucleotide second messengers and T-lymphocyte calcium signaling. *Front Immunol*. 2013; 4: 259. doi: [10.3389/fimmu.2013.00259](#) PMID: [24009611](#)

42. De Flora A, Guida L, Franco L, Zocchi E. The CD38/cyclic ADP-ribose system: a topological paradox. *Int J Biochem Cell Biol.* 1997; 29: 1149–1166. PMID: [9438379](#)
43. Shrimp JH, Hu J, Dong M, Wang BS, MacDonald R, Jiang H, et al. Revealing CD38 cellular localization using a cell permeable, mechanism-based fluorescent small-molecule probe. *J Am Chem Soc.* 2014; 136: 5656–5663. doi: [10.1021/ja411046j](#) PMID: [24660829](#)
44. Song EK, Rah SY, Lee YR, Yoo CH, Kim YR, Yeom JH, et al. Connexin-43 hemichannels mediate cyclic ADP-ribose generation and its Ca²⁺-mobilizing activity by NAD⁺/cyclic ADP-ribose transport. *J Biol Chem.* 2011; 286: 44480–44490. doi: [10.1074/jbc.M111.307645](#) PMID: [22033928](#)
45. Xu M, Li XX, Ritter JK, Abais JM, Zhang Y, Li PL. Contribution of NADPH oxidase to membrane CD38 internalization and activation in coronary arterial myocytes. *PLoS One.* 2013; 8: e71212. doi: [10.1371/journal.pone.0071212](#) PMID: [23940720](#)
46. Ribeiro JM, Carloto A, Costas MJ, Cameselle JC. Human placenta hydrolases active on free ADP-ribose: an ADP-sugar pyrophosphatase and a specific ADP-ribose pyrophosphatase. *Biochim Biophys Acta.* 2001; 1526: 86–94. PMID: [11287126](#)
47. Perraud AL, Shen B, Dunn CA, Rippe K, Smith MK, Bessman MJ, et al. NUDT9, a member of the Nudix hydrolase family, is an evolutionarily conserved mitochondrial ADP-ribose pyrophosphatase. *J Biol Chem.* 2003; 278: 1794–1801. PMID: [12427752](#)
48. Carloto A, Costas MJ, Cameselle JC, McLennan AG, Ribeiro JM. The specific, submicromolar-K_m ADP-ribose pyrophosphatase purified from human placenta is enzymically indistinguishable from recombinant NUDT9 protein, including a selectivity for Mn²⁺ as activating cation and increase in K_m for ADP-ribose, both elicited by H₂O₂. *Biochim Biophys Acta.* 2006; 1760: 1545–1551. PMID: [16860484](#)
49. Zha M, Zhong C, Peng Y, Hu H, Ding J. Crystal structures of human NUDT5 reveal insights into the structural basis of the substrate specificity. *J Mol Biol.* 2006; 364: 1021–1033. PMID: [17052728](#)
50. Andreeva A, Howorth D, Chothia C, Kulesha E, Murzin AG. SCOP2 prototype: a new approach to protein structure mining. *Nucleic Acids Res.* 2014; 42: D310–314. doi: [10.1093/nar/gkt1242](#) PMID: [24293656](#)
51. Sillitoe I, Cuff AL, Dessailly BH, Dawson NL, Furnham N, Lee D, et al. New functional families (FunFams) in CATH to improve the mapping of conserved functional sites to 3D structures. *Nucleic Acids Res.* 2013; 41: D490–498. doi: [10.1093/nar/gks1211](#) PMID: [23203873](#)
52. Rodrigues JR, Fernández A, Canales J, Cabezas A, Ribeiro JM, Costas MJ, et al. Characterization of *Danio rerio* Mn²⁺-dependent ADP-ribose/CDP-alcohol diphosphatase, the structural prototype of the ADPRibase-Mn-like protein family. *PLoS One.* 2012; 7: e42249. doi: [10.1371/journal.pone.0042249](#) PMID: [22848751](#)
53. Kiefer F, Arnold K, Kunzli M, Bordoli L, Schwede T. The SWISS-MODEL Repository and associated resources. *Nucleic Acids Res.* 2009; 37: D387–392. doi: [10.1093/nar/gkn750](#) PMID: [18931379](#)
54. Markley JL, Aceti DJ, Bingman CA, Fox BG, Frederick RO, Makino S, et al. The Center for Eukaryotic Structural Genomics. *J Struct Funct Genomics.* 2009; 10: 165–179. doi: [10.1007/s10969-008-9057-4](#) PMID: [19130299](#)
55. Bradford MM. A rapid and sensitive method for the quantitation of microgram quantities of protein utilizing the principle of protein-dye binding. *Anal Biochem.* 1976; 72: 248–254. PMID: [942051](#)
56. Fehrst A. *Structure and Mechanism in Protein Science. A Guide to Enzyme Catalysis and Protein Folding.* New York: W. Freeman & Co.; 1998.
57. Altschul SF, Wootton JC, Gertz EM, Agarwala R, Morgulis A, Schaffer AA, et al. Protein database searches using compositionally adjusted substitution matrices. *FEBS J.* 2005; 272: 5101–5109. PMID: [16218944](#)
58. Pruitt KD, Tatusova T, Brown GR, Maglott DR. NCBI Reference Sequences (RefSeq): current status, new features and genome annotation policy. *Nucleic Acids Res.* 2012; 40: D130–135. doi: [10.1093/nar/gkr1079](#) PMID: [22121212](#)
59. Klabunde T, Sträter N, Fröhlich R, Witzel H, Krebs B. Mechanism of Fe(III)-Zn(II) purple acid phosphatase based on crystal structures. *J Mol Biol.* 1996; 259: 737–748. PMID: [8683579](#)
60. Richter W. 3',5' Cyclic nucleotide phosphodiesterases class III: members, structure, and catalytic mechanism. *Proteins.* 2002; 46: 278–286. PMID: [11835503](#)
61. Mitic N, Smith SJ, Neves A, Guddat LW, Gahan LR, Schenk G. The catalytic mechanisms of binuclear metallohydrolases. *Chem Rev.* 2006; 106: 3338–3363. PMID: [16895331](#)
62. Shenoy AR, Capuder M, Draskovic P, Lamba D, Visweswariah SS, Podobnik M. Structural and biochemical analysis of the Rv0805 cyclic nucleotide phosphodiesterase from *Mycobacterium tuberculosis*. *J Mol Biol.* 2007; 365: 211–225. PMID: [17059828](#)

63. Kim YG, Jeong JH, Ha NC, Kim KJ. Structural and functional analysis of the Lmo2642 cyclic nucleotide phosphodiesterase from *Listeria monocytogenes*. *Proteins*. 2011; 79: 1205–1214. doi: [10.1002/prot.22954](https://doi.org/10.1002/prot.22954) PMID: [21246635](https://pubmed.ncbi.nlm.nih.gov/21246635/)
64. Sievers F, Wilm A, Dineen D, Gibson TJ, Karplus K, Li W, et al. Fast, scalable generation of high-quality protein multiple sequence alignments using Clustal Omega. *Mol Syst Biol*. 2011; 7: 539. doi: [10.1038/msb.2011.75](https://doi.org/10.1038/msb.2011.75) PMID: [21988835](https://pubmed.ncbi.nlm.nih.gov/21988835/)
65. Robert X, Gouet P. Deciphering key features in protein structures with the new ENDScript server. *Nucleic Acids Res*. 2014; 42: W320–324. doi: [10.1093/nar/gku316](https://doi.org/10.1093/nar/gku316) PMID: [24753421](https://pubmed.ncbi.nlm.nih.gov/24753421/)
66. Sali A, Blundell TL. Comparative protein modelling by satisfaction of spatial restraints. *J Mol Biol*. 1993; 234: 779–815. PMID: [8254673](https://pubmed.ncbi.nlm.nih.gov/8254673/)
67. Sanner MF. A component-based software environment for visualizing large macromolecular assemblies. *Structure*. 2005; 13: 447–462. PMID: [15766546](https://pubmed.ncbi.nlm.nih.gov/15766546/)
68. Morris GM, Goodsell DS, Halliday RS, Huey R, Hart WE, Belew RK, et al. Automated docking using a Lamarckian genetic algorithm and an empirical binding free energy function. *J Comput Chem*. 1998; 19: 1639–1662.
69. Swingle MR, Honkanen RE, Ciszak EM. Structural basis for the catalytic activity of human serine/threonine protein phosphatase-5. *J Biol Chem*. 2004; 279: 33992–33999. PMID: [15155720](https://pubmed.ncbi.nlm.nih.gov/15155720/)
70. Hess B, Kutzner C, van der Spoel D, Lindahl E. GROMACS 4: Algorithms for highly efficient, load-balanced, and scalable molecular simulation. *J Chem Theory Comput*. 2008; 4: 435–447.
71. Oostenbrink C, Villa A, Mark AE, van Gunsteren WF. A biomolecular force field based on the free enthalpy of hydration and solvation: the GROMOS force-field parameter sets 53A5 and 53A6. *J Comput Chem*. 2004; 25: 1656–1676. PMID: [15264259](https://pubmed.ncbi.nlm.nih.gov/15264259/)
72. Berendsen HJC, Postma JPM, Van Gunsteren WF, Hermans J. Interaction models for water in relation to protein hydration. In: Pullman B, editor. *Intermolecular Forces*. Dordrecht: Reidel; 1981. p. 331–342.
73. Hess B. P-LINCS: A parallel linear constraint solver for molecular simulation. *J Chem Theory Comput*. 2008; 4: 116–122.
74. Hess B, Bekker H, Berendsen HJC, Fraaije JGEM. LINCS: A linear constraint solver for molecular simulations. *J Comput Chem*. 1997; 18: 1463–1472.
75. Miyamoto S, Kollman PA. SETTLE: An analytical version of the SHAKE and RATTLE algorithm for rigid water models. *J Comput Chem*. 1992; 13: 952–962.
76. Berendsen HJC, Postma JPM, Van Gunsteren WF, DiNola A, Haak JR. Molecular-dynamics with coupling to an external bath. *J Chem Phys*. 1984; 81: 3684–3690.
77. Kukimoto I, Hoshino S, Kontani K, Inageda K, Nishina H, Takahashi K, et al. Stimulation of ADP-ribosyl cyclase activity of the cell surface antigen CD38 by zinc ions resulting from inhibition of its NAD⁺ glycohydrolase activity. *Eur J Biochem*. 1996; 239: 177–182. PMID: [8706705](https://pubmed.ncbi.nlm.nih.gov/8706705/)
78. Zhuo S, Clemens JC, Stone RL, Dixon JE. Mutational analysis of a Ser/Thr phosphatase. Identification of residues important in phosphoesterase substrate binding and catalysis. *J Biol Chem*. 1994; 269: 26234–26238. PMID: [7929339](https://pubmed.ncbi.nlm.nih.gov/7929339/)
79. Mertz P, Yu L, Sikkink R, Rusnak F. Kinetic and spectroscopic analyses of mutants of a conserved histidine in the metallophosphatases calcineurin and lambda protein phosphatase. *J Biol Chem*. 1997; 272: 21296–21302. PMID: [9261141](https://pubmed.ncbi.nlm.nih.gov/9261141/)
80. Funhoff EG, Wang Y, Andersson G, Averill BA. Substrate positioning by His92 is important in catalysis by purple acid phosphatase. *FEBS J*. 2005; 272: 2968–2977. PMID: [15955057](https://pubmed.ncbi.nlm.nih.gov/15955057/)
81. Keppetipola N, Shuman S. A phosphate-binding histidine of binuclear metallophosphodiesterase enzymes is a determinant of 2',3'-cyclic nucleotide phosphodiesterase activity. *J Biol Chem*. 2008; 283: 30942–30949. doi: [10.1074/jbc.M805064200](https://doi.org/10.1074/jbc.M805064200) PMID: [18757371](https://pubmed.ncbi.nlm.nih.gov/18757371/)
82. Rao F, Qi Y, Murugan E, Pasunooti S, Ji Q. 2',3'-cAMP hydrolysis by metal-dependent phosphodiesterases containing DHH, EAL, and HD domains is non-specific: Implications for PDE screening. *Biochem Biophys Res Commun*. 2010; 398: 500–505. doi: [10.1016/j.bbrc.2010.06.107](https://doi.org/10.1016/j.bbrc.2010.06.107) PMID: [20599695](https://pubmed.ncbi.nlm.nih.gov/20599695/)
83. Graeff R, Liu Q, Kriksunov IA, Kotaka M, Oppenheimer N, Hao Q, et al. Mechanism of cyclizing NAD to cyclic ADP-ribose by ADP-ribosyl cyclase and CD38. *J Biol Chem*. 2009; 284: 27629–27636. doi: [10.1074/jbc.M109.030965](https://doi.org/10.1074/jbc.M109.030965) PMID: [19640843](https://pubmed.ncbi.nlm.nih.gov/19640843/)